Supporting Information

Structure and Dynamics of Uranyl(VI) and Plutonyl(VI) Cations in Ionic Liquid/Water Mixtures via Molecular Dynamics Simulations

Katie A. Maerzke,[†] George S. Goff,[‡] Wolfgang H. Runde,[‡]
William F. Schneider[†,§] and Edward J. Maginn[†,∗]

Department of Chemical and Biomolecular Engineering, University of Notre Dame,
Notre Dame, IN 46556 USA

Chemistry Division, Los Alamos National Laboratory, Los Alamos, NM 87545 USA

Department of Chemistry and Biochemistry, University of Notre Dame,
Notre Dame, IN 46556 USA

Abstract

A fundamental understanding of the behavior of actinides in ionic liquids is required to develop advanced separation technologies. Spectroscopic measurements indicate a change in the coordination of uranyl in the hydrophobic ionic liquid 1-ethyl-3-methylimidazolium bis(trifluoromethylsulfonyl)imide ([EMIM][Tf$_2$N]) as water is added to the system. Molecular dynamics simulation of dilute uranyl (UO$_2^{2+}$) and plutonyl (PuO$_2^{2+}$) solutions in [EMIM][Tf$_2$N]/water mixtures have been performed in order to examine the molecular-level coordination and dynamics of the actinyl cation (AnO$_2^{2+}$; An = U, Pu) as the amount of water in the system changes. The simulations show that the actinyl cation has a strong preference for a first solvation shell with five oxygen atoms, although a higher coordination number is possible in mixtures with little or no water. Water is a much stronger ligand for the actinyl cation than Tf$_2$N, with even very small amounts of water displacing Tf$_2$N from the first solvation shell. When enough water is present, the inner coordination sphere of each actinyl cation contains five water molecules without any Tf$_2$N. Water also populates the second solvation shell, although it does not completely displace the Tf$_2$N. At high water concentrations a significant fraction of the water is found in the bulk ionic liquid, where it primarily coordinates with the Tf$_2$N anion. Potential of mean force simulations show that the progressive addition of up to five water molecules to uranyl is very favorable, with ΔG ranging from -52.3 kJ/mol for the addition of the first water molecule to -37.6 kJ/mol for the addition of the fifth. Uranyl and plutonyl dimers formed via bridging Tf$_2$N ligands are found in [EMIM][Tf$_2$N] and in mixtures with very small amounts of water. Potential of mean force calculations confirm that the dimeric complexes are stable, with relative free energies of up to -9 kJ/mol in pure [EMIM][Tf$_2$N]. We find that the self-diffusion coefficients for all the components in the mixture increase as the water content increases, with the largest increase for water and the smallest increase for the ionic liquid cation and anion. The velocity autocorrelation functions also indicate changes in structure and dynamics as the water content changes.

[†]University of Notre Dame, Department of Chemical and Biomolecular Engineering
[‡]Los Alamos National Laboratory
[§]University of Notre Dame, Department of Chemistry and Biochemistry
[∗]Corresponding author. Email: ed@nd.edu

Acknowledgements

Supporting Information Contents

The details of the simulations, along with a figure showing the MSD for uranyl at 400 and 298 K and a table with the average temperature and pressure over the course of the 15 ns NVE production run are available in the Supporting Information. Also available are a table with the position of the first maximum of the An-O(H_2O) and An-O(Tf$_2$N) radial distribution functions, a figure showing U-O(Tf$_2$N), U-N(Tf$_2$N), and U-N(EMIM) RDFs, a table with the average bond lengths and angles for the actinyl cations, and a figure showing simulation snapshots of the water molecules in the first solvation shell for uranyl cations with different coordination environments. Additionally, figures showing the H(H_2O)-O(Tf$_2$N) and H(H_2O)-O(H_2O) RDFs and the axial oxygen-water hydrogen RDFs and NIs, simulation snapshots showing the location of the water molecules in the first and second solvation shell of uranyl cations, and a figure showing the actinide-actinide RDFs for the different independent simulations, a figure showing the intramolecular oxygen-oxygen distances in Tf$_2$N, and a figure showing Tf$_2$N-Tf$_2$N, Tf$_2$N-EMIM, and EMIM-EMIM RDFs are included. Finally, figures showing the MSD and VACF of the ionic liquid cation and anion can be found in the Supporting Information.

Simulation Details

The functional form of the force fields in this work is given by

$$U_{\text{tot}} = \sum_{\text{bonds}} k_r \left(r - r_0 \right)^2 + \sum_{\text{angles}} k_\theta \left(\theta - \theta_0 \right)^2 + \tag{1}$$

$$\sum_{\text{dihedrals}} k_\chi \left[1 + \cos(n\chi - \delta) \right] + \tag{2}$$

$$\sum_{\text{pairs}} \left\{ 4\epsilon_{ij} \left[\left(\frac{\sigma_{ij}}{r_{ij}} \right)^{12} - \left(\frac{\sigma_{ij}}{r_{ij}} \right)^6 \right] + \frac{q_i q_j}{r_{ij}} \right\} \tag{3}$$

where the total energy is expressed in terms of bond stretching, angle bending, dihedral rotations (including improper dihedrals for the imidazolium ring), and pairwise non-bonded interactions represented using the Lennard-Jones and Coulomb potentials. The unlike Lennard-Jones parameters

are determined using the Lorentz-Berthelot combining rules:[1]

$$\sigma_{ij} = \frac{1}{2}\left(\sigma_{ii} + \sigma_{jj}\right) \quad \text{and} \quad \epsilon_{ij} = \left(\epsilon_{ii}\epsilon_{jj}\right)^{1/2}$$

The molecular dynamics simulation package GROMACS 4.5.5[2–5] was used for all MD simulations. The simulations were performed in a cubic box with periodic boundaries in all directions. The Leapfrog algorithm[6] with a 2 fs time step was used to integrate the equations of motion. A 1.20 nm cut-off with a switching function from 1.18 to 1.20 nm with a neighbor list cut-off of 1.50 nm was used for the non-bonded (LJ + Coulomb) interactions. The Coulomb potential was calculated using the particle mesh Ewald method[7,8] with a Fourier grid spacing of 0.12 nm in reciprocal space. The rigid water model was constrained using SETTLE[9] and the hydrogen bonds in the imidazolium ring were constrained using parallel LINCS.[10,11] Initial random configurations were generated using Packmol.[12] The initial configurations were then relaxed through steepest descent energy minimization, followed by 1 ns of MD simulation in the canonical (NVT) ensemble at 700 K with the Berendsen thermostat[13] having a time constant of 0.5 ps. This was followed by another 1 ns run in the isothermal-isobaric (NpT) ensemble at 700 K and 1 atm. These initial short runs at 700 K were necessary to obtain a reasonable starting structure. The system was then annealed for 2 ns in the NpT ensemble to reach the target temperature of 400 K. At this point the system was equilibrated for 20 ns in the NpT ensemble using a Nosé-Hoover thermostat[14,15] and Parrinello-Rahman barostat[16,17] with time constants of 3.0 ps for both the thermostat and barostat. Next followed 5 ns simulation in the NVT ensemble with the density fixed at the average value from the last 10 ns of NpT equilibration. This was followed by a production run of 15 ns in the NVE ensemble using the double precision version of GROMACS to ensure conservation of energy with a nominal temperature and pressure of 400 K and 1 atm. Positions were written out every 1000 steps or 2 ps for later analysis. Average temperatures and pressures over the NVE run are available in Table S1 of the Supporting Information. 15 ns NVE takes about 2 days on 12 shared-memory processors

In addition, umbrella sampling[18,19] simulations were run to calculate potentials of mean force[20] for the progressive addition of water molecules to uranyl in [EMIM][Tf$_2$N], the displacement of water by Tf$_2$N for uranyl with five water molecules, the addition of a sixth water molecule to five-coordinate plutonyl, and for the association of actinyl cations in [EMIM][Tf$_2$N] with and without small amounts of water. For these simulations a smaller system size of 80 [EMIM][Tf$_2$N] ion pairs with a single actinyl cation and a $1-8$ water molecules was used, resulting in a simulation box length of approximately 3.35 nm. The initial configurations were equilibrated using the same annealing procedure outlined above, followed by a 10 ns equilibration run in the NpT ensemble at 400 K and 1 atm using the Nosé-Hoover thermostat and Parrinello-Rahman barostat. Statistics for the potential of mean force were then collected over a 25 ns NpT run with the positions and

forces for the constrained molecules written every 1000 steps (2 ps). The force constants for the harmonic umbrella potential ranged from $100,000$ to $20,000$ kJ/mol/nm^2, with the larger values for the shorter distances. Simulations were performed every 0.02 nm along a given reaction coordinate, with a smaller spacing of 0.01 nm from 0.23 to 0.28 nm (near the minimum). The PMF was extracted from the simulations using the weighted histogram analysis method (WHAM)[21–23] as implemented in the GROMACS analysis routine g_wham.[24]

At each concentration and for each point along the PMF, two independent simulations were performed in order to obtain more reliable statistics. The actinyl Tf$_2$N complexes were initialized as both associated [AnO$_2$(Tf$_2$N)$_2$]$^{+0.4}$ and dissociated AnO$_2^{2+}$ + 2 Tf$_2$N$^{-0.8}$. For the systems with the smallest amount of water (0.95 and 0.90 mole fraction IL), an additional six independent simulations (for a total of eight) were performed to obtain sufficient sampling at these concentrations. An additional two independent simulations were performed for the pure IL systems to obtain better sampling of the association between the actinyl cations. The reported uncertainties are the standard deviation calculated from the average of each indepedent simulation. The MD trajectories were analyzed using a combination of the GROMACS analysis routines and custom in-house analysis code.
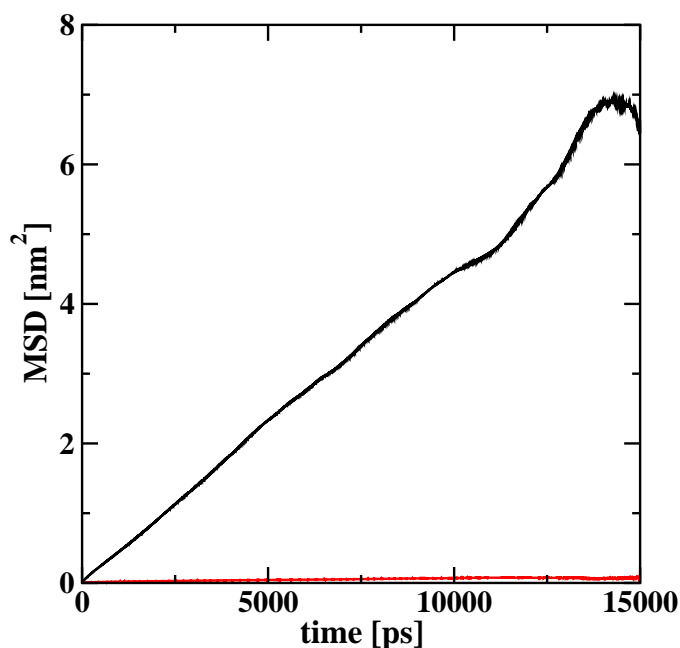

Figure S1: Center of mass mean square displacement for uranyl in [EMIM][Tf$_2$N] without any water at 400 K (black) and 298 K (red)

Table S1: Average temperature and pressure over the course of the 15 ns NVE production run.[a]

	UO$_2$		PuO$_2$	
x_{IL}	T [K]	p [atm]	T [K]	p [atm]
1.00	398_2	-17_{14}	399_1	-5_{38}
0.95	401_3	13_{23}	398_2	-17_{21}
0.90	401_2	12_{22}	402_3	20_{25}
0.85	400_1	7_5	401_3	19_{24}
0.81	397_1	-23_{12}	400_1	3_1
0.77	402_1	19_6	397_1	-23_3
0.74	401_1	13_{11}	401_1	13_9
0.71	402_2	17_{18}	400_1	5_6

[a]Subscripts indicate uncertainties in the final digit.

Results and Discussion

Table S2: The position (in nm) of the maximum in the first peak of the An-O RDF for the oxygen atom in water and Tf$_2$N.[a]

	An-O(H$_2$O)		An-O(Tf$_2$N)	
x_{IL}	UO$_2$	PuO$_2$	UO$_2$	PuO$_2$
1.00	–	–	0.251	0.251
0.95	0.243	0.245	0.251	0.251
0.90	0.245	0.247	0.257	0.255
0.85	0.247	0.247	–	–
0.81	0.247	0.247	–	–
0.77	0.247	0.247	–	–
0.74	0.245	0.247	–	–
0.71	0.245	0.247	–	–

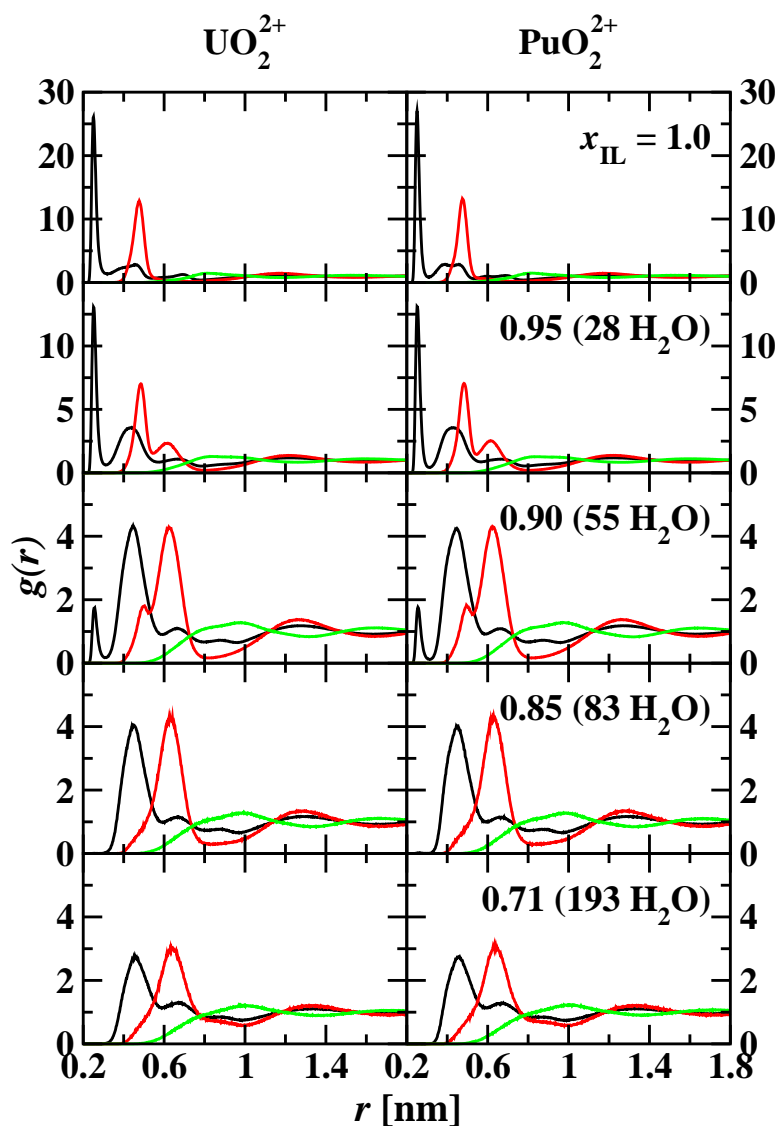[a]Subscripts indicate uncertainties in the final digit.

Figure S2: U-O(Tf$_2$N) (black), U-N(Tf$_2$N) (red), and U-N(EMIM) (green) radial distribution functions in mixtures with uranyl (left) and plutonyl (right) at 1.0, 0.95, 0.90, 0.85, and 0.71 mole fraction IL. Mixtures at 0.81, 0.77, and 0.74 mole fraction IL not shown as there is not much difference between 0.85 and 0.71 mole fraction IL. Note that the U-N(Tf$_2$N) peak is shifted relative to the U-O(Tf$_2$N) peak; this is a result of the elongated nature of the molecule, where the intramolecular distance between O and N atoms is more than 0.2 nm.

Table S3: Average bond lengths and angles for the actinyl cations.[a]

| | UO_2 | | PuO_2 | |
x_{IL}	bond length [nm]	bend angle [deg]	bond length [nm]	bend angle [deg]
1.00	0.1772	166.14_7	0.1710	173.68_2
0.95	0.1774	169.4_2	0.1712	174.13_3
0.90	0.1775	171.19_4	0.1714	174.42_2
0.85	0.1776	171.43_2	0.1715	174.49_2
0.81	0.1776	171.40_3	0.1715	174.51_1
0.77	0.1776	171.32_1	0.1715	174.53_1
0.74	0.1776	171.29_1	0.1715	174.50_1
0.71	0.1776	171.25_2	0.1715	174.50_1

[a]Subscripts indicate uncertainties in the final digit.
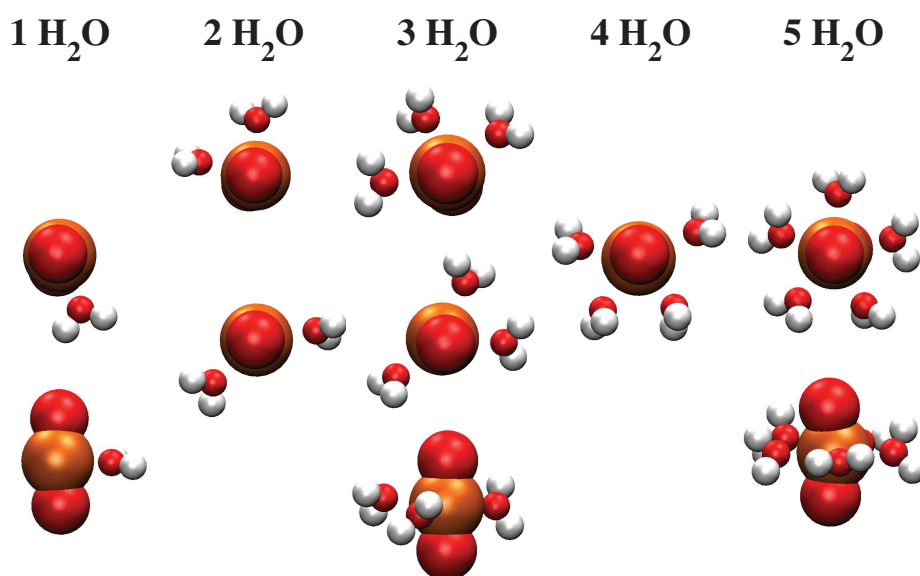
Figure S3: Simulation snapshots showing the water molecules in the first solvation shell of uranyl for coordination environments with 1–5 water molecules. The Tf_2N anions have been removed for clarity.
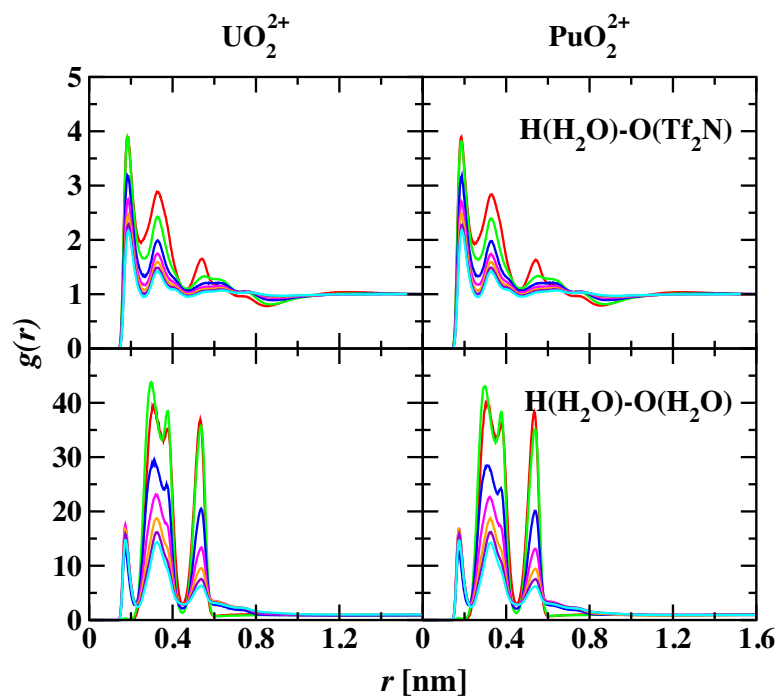
Figure S4: H(H$_2$O)-O(Tf$_2$N) (top) and H(H$_2$O)-O(H$_2$O) (bottom) radial distribution functions in mixtures with uranyl (left) and plutonyl (right). 1.0 mole fraction IL (black), 0.95 (red), 0.90 (green), 0.85 (blue), 0.81 (magenta), 0.77 (orange), 0.74 (violet), and 0.71 (cyan).
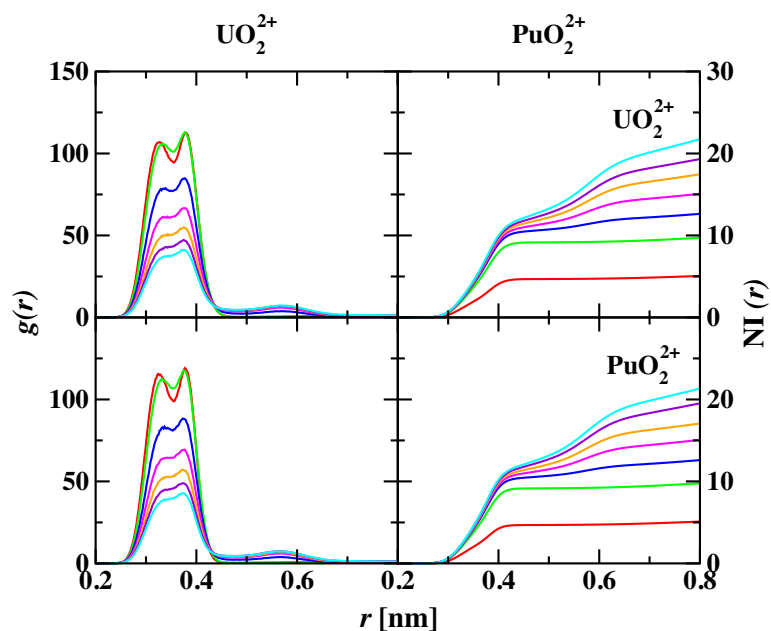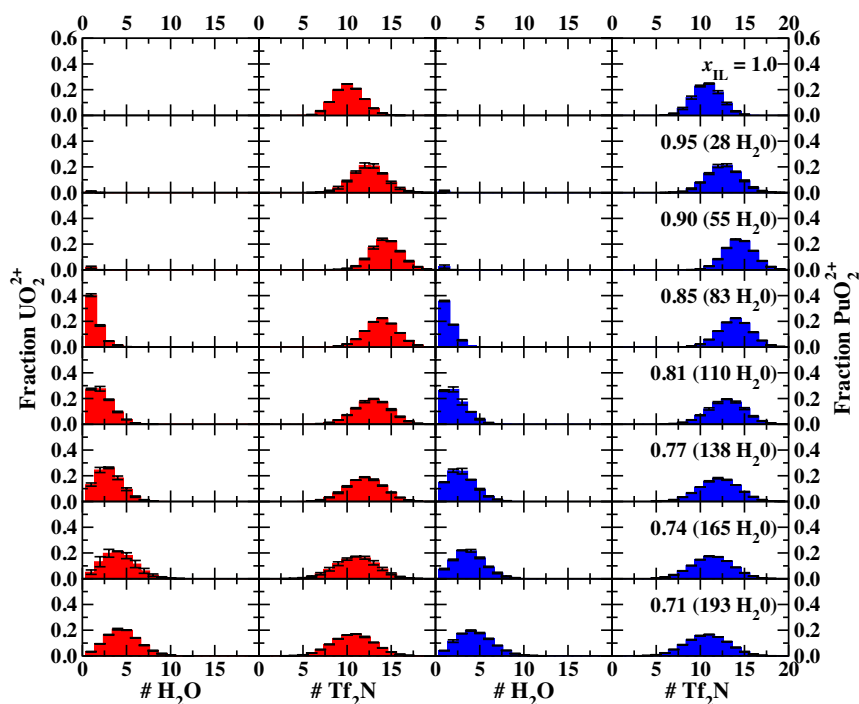

Figure S5: O(AnO$_2$)-H(H$_2$O) radial distribution functions (left) and number integrals (right) in mixtures with uranyl (top) and plutonyl (bottom). 1.0 mole fraction IL (black), 0.95 (red), 0.90 (green), 0.85 (blue), 0.81 (magenta), 0.77 (orange), 0.74 (violet), and 0.71 (cyan).

Figure S6: Distribution of the coordination numbers of water (left) and Tf$_2$N (right) oxygen atoms with UO$_2^{2+}$ (red, left) and PuO$_2^{2+}$ (blue, right) in the second solvation shell. Note that the definition of the second solvation shell is somewhat ill-defined (see the number integrals in Figure 2). The error bars indicate the standard deviation.
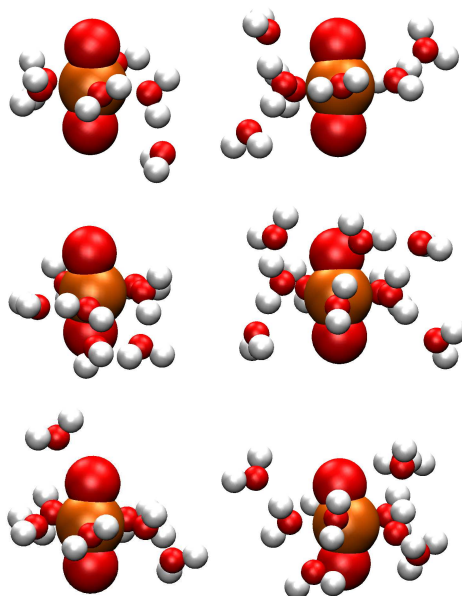

Figure S7: Simulation snapshots showing the water molecules in the first and second solvation shell of uranyl. The Tf$_2$N anions have been removed for clarity.
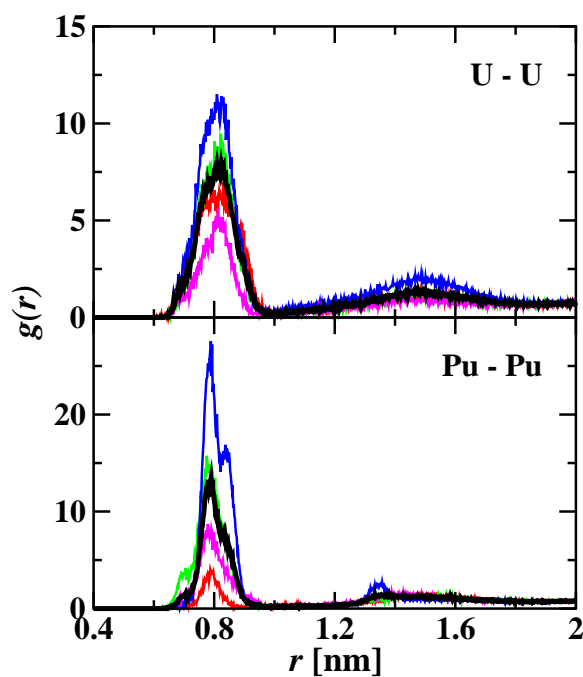
Figure S8: U-U (top) and Pu-Pu (bottom) radial distribution functions in the pure IL system. The colored lines indicate the different independent simulations and the thick black line is the average.
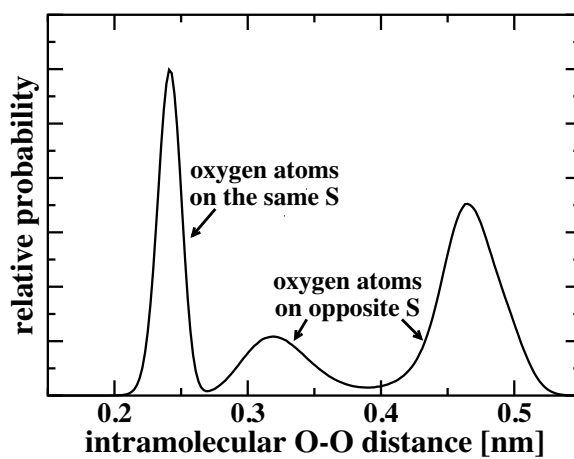

Figure S9: Intramolecular oxygen-oxygen distances of Tf_2N in [EMIM][Tf_2N] solution.

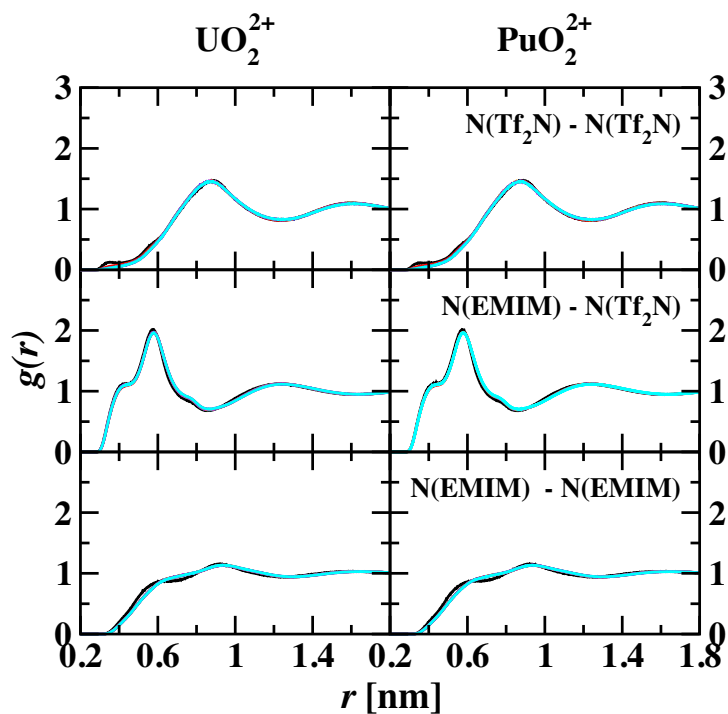**Figure S10:** N(Tf$_2$N)-N(Tf$_2$N), N(EMIM)-N(Tf$_2$N), and N(EMIM)-N(EMIM) radial distribution functions in mixtures with uranyl (left) and plutonyl (right). 1.0 mole fraction IL (black), 0.95 (red), 0.90 (green), 0.85 (blue), 0.81 (magenta), 0.77 (orange), 0.74 (violet), and 0.71 (cyan).

Figure S11: Residence time correlation for the actinyl cation with water (top) and Tf$_2$N (bottom) in the second solvation shell for uranyl (left) and plutonyl (right). 1.0 mole fraction IL (black), 0.95 (red), 0.90 (green), 0.85 (blue), 0.81 (magenta), 0.77 (orange), 0.74 (violet), and 0.71 (cyan).
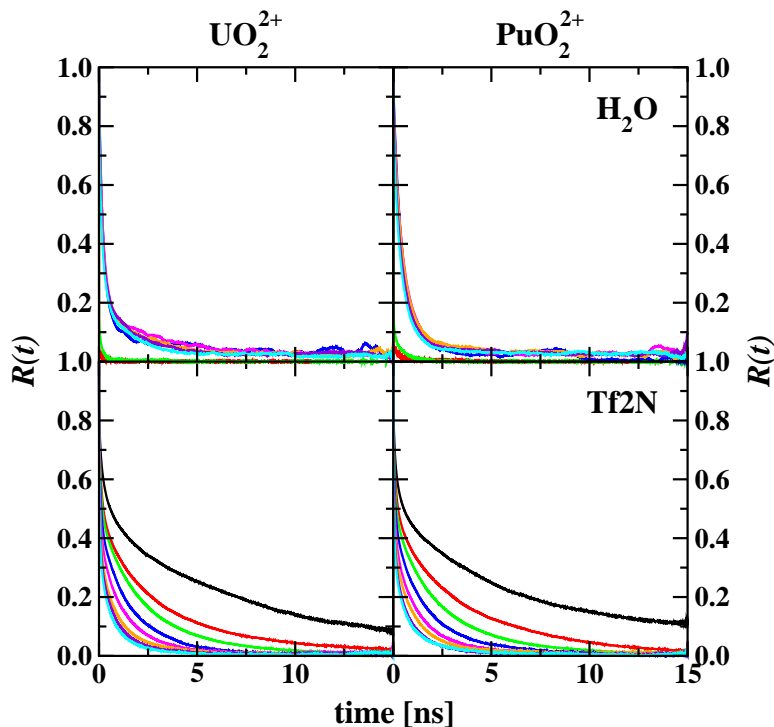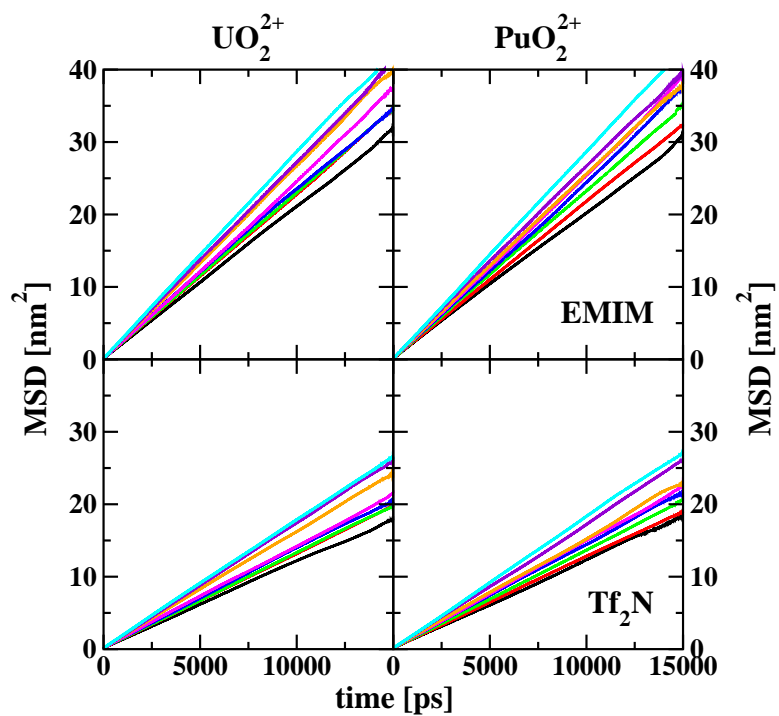
11

Figure S12: Center of mass mean square displacement for EMIM (top) and Tf_2N (bottom) in systems with uranyl (left) and plutonyl (right) in water/IL mixtures. 1.0 mole fraction IL (black), 0.95 (red), 0.90 (green), 0.85 (blue), 0.81 (magenta), 0.77 (orange), 0.74 (violet), and 0.71 (cyan).
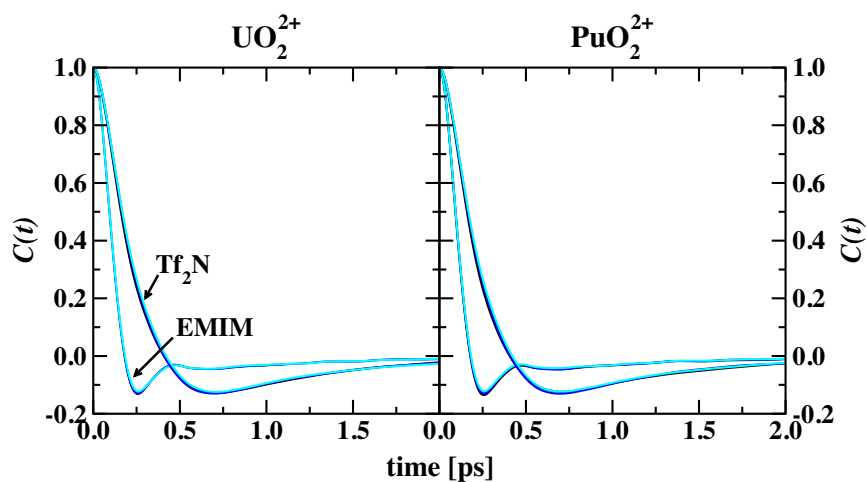

Figure S13: Center of mass velocity autocorrelation function for EMIM and Tf_2N in systems with uranyl (left) and plutonyl (right) in water/IL mixtures. For clarity, only select mole fractions are shown. 1.0 mole fraction IL (black), 0.85 (blue), and 0.71 (cyan).

References

[1] Maitland, G. C.; Rigby, M.; Smith, E. B.; Wakeham, A. *Intermolecular Forces: Their Origin and Determination*; Pergamon Press: Oxford, 1987.

[2] Hess, B.; Kutzner, C.; van der Spoel, D.; Lindahl, E. GROMACS 4: Algorithms for Highly Efficient, Load-Balanced, and Scalable Molecular Simulation. *J. Chem. Theory Comput.* **2008**, *4*, 435–447.

[3] van der Spoel, D.; Lindahl, E.; Hess, B.; Groenhof, G.; Mark, A. E.; Berendsen, H. J. C. GROMACS: Fast, Flexible, and Free. *J. Comp. Chem.* **2005**, *26*, 1701–1719.

[4] Lindahl, E.; Hess, B.; van der Spoel, D. GROMACS 3.0: A Package for Molecular Simulation and Trajectory Analysis. *J. Mol. Mod.* **2001**, *7*, 306–317.

[5] Berendsen, H. J. C.; van der Spoel, D.; van Drunen, R. GROMACS: A Message-Passing Parallel Molecular Dynamics Implementation. *Comp. Phys. Comm.* **1995**, *91*, 43–56.

[6] Hockney, R. W.; Goel, S. P.; Eastwood, J. Quiet High Resolution Computer Models and a Plasma. *J. Comp. Phys.* **1974**, *14*, 148–158.

[7] Darden, T.; York, D.; Pedersen, L. Particle Mesh Ewald: An $N \log(N)$ Method for Ewald Sums in Large Systems. *J. Chem. Phys.* **1993**, *98*, 10089–10092.

[8] Essmann, U.; Perera, L.; Berkowitz, M. L.; Darden, T.; Lee, H.; Pedersen, L. A Smooth Particle Mesh Ewald Potential. *J. Chem. Phys.* **1995**, *103*, 8577–8592.

[9] Miyamoto, S.; Kollman, P. A. SETTLE: An Analytical Version of the SHAKE and RATTLE Algorithms for Rigid Water Models. *J. Comp. Chem.* **1992**, *13*, 952–962.

[10] Hess, B.; Bekker, H.; Berendsen, H. J. C.; Fraaije, J. G. E. M. LINCS: A Linear Constraint Solver for Molecular Simulations. *J. Comp. Chem.* **1997**, *18*, 1463–1472.

[11] Hess, B. P-LINCS: A Parallel Linear Constraint Solver for Molecular Simulation. *J. Chem. Theory Comput.* **2008**, *4*, 116–122.

[12] Martínez, L.; Andrade, R.; Birgin, E. G.; Martínez, J. M. Packmol: A Package for Building Initial Configurations for Molecular Dynamics Simulations. *J. Comp. Chem.* **2009**, *30*, 2157–2164.

[13] Berendsen, H. J. C.; Postma, J. P. M.; DiNola, A.; Haak, J. R. Molecular Dynamics with Coupling to an External Bath. *J. Chem. Phys.* **1984**, *81*, 3684–3690.

[14] Nosé, S. A Molecular Dynamics Method for Simulations in the Canonical Ensemble. *Mol. Phys.* **1984**, *52*, 255–268.

[15] Hoover, W. G. Canonical Dynamics: Equilibrium Phase-Space Distributions. *Phys. Rev. A* **1985**, *31*, 1695–1697.

[16] Parrinello, M.; Rahman, A. Polymorphic Transitions in Single Crystals: A New Molecular Dynamics Method. *J. Appl. Phys.* **1981**, *52*, 7182–7190.

[17] Nosé, S.; Klein, M. L. Constant Pressure Molecular Dynamics for Molecular Systems. *Mol. Phys.* **1983**, *50*, 1055–1076.

[18] Torrie, G. M.; Valleau, J. P. Monte Carlo Free Energy Estimates Using Non-Boltzmann Sampling - Application to Subcritical Lennard-Jones Fluid. *Chem. Phys. Lett.* **1974**, *28*, 578–581.

[19] Torrie, G. M.; Valleau, J. P. Nonphysical Sampling Distributions in Monte Carlo Free-Energy Estimation: Umbrella Sampling. *J. Comp. Phys.* **1977**, *23*, 187–199.

[20] Kirkwood, J. G. Statistical Mechanics of Fluid Mixtures. *J. Chem. Phys.* **1935**, *3*, 300–313.

[21] Kumar, S.; Bouzida, D.; Swendsen, R. H.; Kollman, P. A.; Rosenberg, J. M. The Weighted Histogram Analysis Method for Free Energy Calculation on Biomolecules 1. The Method. *J. Comput. Chem.* **1992**, *13*, 1011–1021.

[22] Ferrenberg, A. M.; Swendsen, R. H. New Monte Carlo Technique for Studying Phase Transitions. *Phys. Rev. Lett.* **1988**, *61*, 2635–2638.

[23] Ferrenberg, A. M.; Swendsen, R. H. Optimized Monte Carlo Data Analysis. *Phys. Rev. Lett.* **1989**, *63*, 1195–1198.

[24] Hub, J. S.; de Groot, B. L.; van der Spoel, D. g_wham–A Free Weighted Histogram Analysis Implementation Including Robust Error and Autocorrelation Estimates. *J. Chem. Theory Comput.* **2010**, *6*, 3713–3720.